Society For Biomaterials

Efficacy of a synthetic calcium phosphate with submicron surface topography as autograft extender in lapine posterolateral spinal fusion

Lukas A. van Dijk,[1,2§] **Davide Barbieri**,[1§] **Florence Barrère-de Groot**,[1] **Huipin Yuan**,[1,3] **Rema Oliver**,[4] **Chris Christou**,[4] **William R. Walsh**,[4] **Joost D. de Bruijn**[1,5]

[1]Kuros Biosciences BV, Bilthoven, the Netherlands
[2]Department of Oral and Maxillofacial Surgery, University Medical Center Utrecht, Utrecht, the Netherlands
[3]Complex Tissue Regeneration, MERLN Institute, Maastricht University, Maastricht, the Netherlands
[4]Surgical and Orthopedic Research Laboratories, University of New South Wales, Sydney, New South Wales, Australia
[5]School of Engineering and Materials Science, Queen Mary University of London, London, UK

Received 13 September 2018; revised 18 November 2018; accepted 1 December 2018
Published online 7 January 2019 in Wiley Online Library (wileyonlinelibrary.com). DOI: 10.1002/jbm.b.34301

Abstract: Posterolateral spinal fusion (PLF) is a common procedure in orthopedic surgery that is performed to fuse adjacent vertebrae to reduce symptoms related to spinal conditions. In the current study, a novel synthetic calcium phosphate with submicron surface topography was evaluated as an autograft extender in a validated rabbit model of PLF. Fifty-nine skeletally mature New Zealand white rabbits were divided into three groups and underwent single-level intertransverse process PLF at L4-5 using (1) autologous bone graft (ABG) alone or in a 1:1 combination with (2) calcium phosphate granules (ABG/$BCP_{granules}$), or (3) granules embedded in a fast-resorbing polymeric carrier (ABG/BCP_{putty}). After 6, 9, and 12 weeks, animals were sacrificed and spinal fusion was assessed by manual palpation, Radiographs, micro-CT, mechanical testing (12 weeks only), histology, and histomorphometry. Based on all endpoints, all groups showed a gradual progression in bone formation and maturation during time, leading to solid fusion masses between the transverse processes after 12 weeks. Fusion assessments by manual palpation, radiography and histology were consistent and demonstrated equivalent fusion rates between groups, with high bilateral fusion rates after 12 weeks. Mechanical tests after 12 weeks indicated substantially lower range of motion for all groups, compared to non-operated controls. By histology and histomorphometry, the gradual formation and maturation of bone in the fusion mass was confirmed for each graft type. With these results, we describe the equivalent performance between autograft and a novel calcium phosphate material as an autograft extender in a rabbit model of PLF using an extensive range of evaluation techniques. © 2019 The Authors. *Journal of Biomedical Materials Research Part B: Applied Biomaterials* published by Wiley Periodicals, Inc. J Biomed Mater Res Part B: Appl Biomater 107B:2080–2090, 2019.

Key Words: posterolateral spinal fusion, rabbit, calcium phosphate, submicron surface topography

How to cite this article: van Dijk LA, Barbieri D, Barrère-de Groot F, Yuan H, Oliver R, Christou C, Walsh WR, de Bruijn JD. 2019. Efficacy of a synthetic calcium phosphate with submicron surface topography as autograft extender in lapine posterolateral spinal fusion. J Biomed Mater Res Part B 2019:107B:2080–2090.

INTRODUCTION

Spinal fusion is a frequent procedure in orthopedic surgery, which is performed to fuse vertebrae of the spine to improve symptoms resulting from spinal trauma, degenerative conditions, scoliosis or tumor resections. The posterolateral spinal fusion (PLF) technique is commonly performed in the lumbar spine and involves bilateral implantation of bone graft between the transverse processes of adjacent vertebrae. Although autologous bone is the gold standard graft for spinal fusion procedures, pseudoarthrosis and non-unions are still frequently reported complications of this treatment.[1–6] Moreover, the required harvesting of large autograft volumes, usually obtained from the iliac crest, leads to morbidity[7,8] and persistent post-surgical pain in up to 60% of patients.[2]

In order to improve the fusion rate of PLF procedures and to reduce the amount of bone autograft to be harvested, there has been an increasing interest in calcium phosphate materials that can support spinal bone formation as autograft extenders.[9,10] Synthetic calcium phosphates are generally osteoconductive and highly biocompatible, making them suitable biomaterials for use in bone surgery. As mere osteoconductive materials, their regenerative potential is limited and the presence of an osteogenic or osteoinductive adjunct is favored for bone growth to occur. However, a subset of calcium phosphates with optimized physicochemical properties was demonstrated to have exceptional

The copyright line for this article was changed on Aug 5, 2019 after original online publication.
[§]These authors contributed equally to this work.
Correspondence to: J. D. de Bruijn; e-mail: j.d.debruijn@qmul.ac.uk
Contract grant sponsor: European Union's Horizon 2020 research and innovation program; contract grant number: 674282

bone-inducing properties on its own,[11–13] showing enhanced regenerative performance in pre-clinical studies.[11–14] Specifically, the presence of a submicron surface topography was related to the enhanced bone-inducing potential of these calcium phosphates.[11,13–15] Interestingly, studies have demonstrated that surface properties of biomaterials can influence the phenotype of macrophages,[16–18] immune cells that govern the foreign body response and wound healing response.[19] An increase in anti-inflammatory M2 macrophages following an initial inflammatory phase has been shown to be beneficial for bone formation[20] and vascularization[21] and recently, macrophages cultured on calcium phosphates with submicron surface topography were demonstrated to adopt the M2 phenotype.[22] This suggests a connection between surface topography, macrophage phenotype and the enhanced vascularization[22] and bone formation observed with submicron surface structured calcium phosphates *in vivo.*

The current study describes the evaluation of a novel synthetic calcium phosphate with surface topography consisting of submicron polygon crystals in a validated rabbit model of PLF, which is well-described for studies of autograft extender efficacy.[23–26] Either in granular form or as granules embedded within a fast-resorbing polymeric carrier material designed to improve handling properties, the calcium phosphate was combined with iliac crest-derived bone graft in a 1:1 ratio, after which the graft composites were implanted. Study outcomes included fusion rate by manual palpation, radiography, micro-computed tomography and histology at 6, 9, and 12 weeks post-surgery. Furthermore, biomechanical analysis of the spines and histomorphometry of bone and material in the fusion mass were performed.

MATERIALS AND METHODS

Graft materials

Calcium phosphate granules. Commercially available biphasic calcium phosphate (BCP) bone graft (MagnetOs; Kuros Biosciences) was provided in granule and putty formulations. Both formulations contained 1–2 mm granules of bioactive bone graft comprising 65–75% Tri-Calcium Phosphate (TCP – $Ca_3(PO_4)_2$) and 25–35% Hydroxyapatite (HA – $Ca_{10}(PO_4)_6{\cdot}(OH)_2$). The granules were manufactured from porous BCP blocks produced by use of calcium orthophosphate powder, foaming agent and porogen. Blocks were dried, sintered and crushed to obtain granules (1–2 mm) which were subsequently exposed to a hydrothermal treatment to create submicron surface topography [Fig. 1(A)]. Submicron size of surface crystals was confirmed by scanning electron microscopy (SEM, JEOL JSM-5600, JEOL Ltd, Tokyo, Japan), revealing an average crystal diameter of 0.58 ± 0.21 μm.

Polymeric carrier. For the putty formulation, a tri-block copolymer was synthesized from polyethylene glycol (PEG, 80–90 mol %) and L-lactide monomer (10–20 mol %), with a molecular weight of 2–3 kDa. The resulting polymer is water-soluble and dissolves near body temperature, leading to rapid dispersion after implantation (<48 h). The BCP granules and binder were combined to obtain a moldable putty. The materials were sterilized by gamma irradiation (25 kGy).

Autologous bone graft and graft composites. The iliac crests were exposed from the caudal aspect of the midline incision used to approach the spine. Corticocancellous bone was harvested from both iliac crests using a Miltex Rongeur. Volume and weight of the autologous bone graft (ABG) particles (< 5 mm in size) was measured in a 3 mL syringe (tip removed) and a laboratory balance [Fig. 1(B)]. A volume of 1 cc (~0.8 g) of autograft particles was combined with 1 cc of BCP granules ($ABG/BCP_{granules}$) [Fig. 1(C,D)]. Likewise, 1 cc of autograft particles was combined with 1 cc of putty (ABG/BCP_{putty}) [Fig. 1(E,F)]. Volumes of 2 cc of ABG, $ABG/BCP_{granules}$ and ABG/BCP_{putty} were determined for implantation on each side of the spine (4 cc total per level). A volume of 2 cc of autograft per side is known to achieve spinal fusion in this rabbit model, as has been reported in literature.[27] Furthermore, a volume of 1 cc of autograft has been reported to be unable to achieve fusion in this model.[28]

Animal model and surgical procedure

After approval of the Institutional Animal Care and Ethics Committee (ACEC approval 14/110A, UNSW, Australia), 54 adult New Zealand white rabbits underwent single-level bilateral posterolateral intertransverse process spine arthrodesis at L4–L5. Skeletal maturity was confirmed prior to being enrolled in the study by radiographic confirmation of the closure of the growth plates of the proximal tibia. The animals were sedated with a mixture of midazolam (5 mg/mL at 0.3–0.5 mg/kg) and buprenorphine (0.326 mg/mL at 0.03–0.05 mg/kg) intramuscularly. Anesthesia was applied and maintained via isoflurane inhalation (2–3%) with oxygen. Once the rabbits were anesthetized, the skin was incised from the L3–L5 levels. The intermuscular plane between the multifidus and longissimus muscles was separated in a blunt fashion to expose the transverse processes as well as the intertransverse membrane. A pneumatic burr (Midax Rex) was used with an M8 matchstick burr to prepare the host bone between the levels by decortication. The transverse processes were carefully decorticated for a distance of 10 mm from the vertebral body and pars to a level where bleeding bone beds were visually present to the surgeon.

The animals were divided into three groups: (1) ABG, (2) $ABG/BCP_{granules}$, and (3) ABG/BCP_{putty}. For each group, a total volume of 2 cc graft material per side (4 cc per level) was implanted between the L4–L5 transverse processes in the paraspinal bed. After implant placement, the muscle layers were allowed to return to their native position and the fascial incisions were closed with 3–0 absorbable sutures and the skin approximated using 3–0 sutures. Post-operative pain was managed using a non-steroid anti-inflammatory drug (Carprofen, 50 mg/mL, dose 2–4 mg/kg) for the first 2–3 days. The animals were housed in individual cages, fed *ad libitum* and monitored daily for the first 7 days following surgery and weekly thereafter. Animals were euthanized at 6 (n = 5), 9 (n = 5), and 12 (n = 8) weeks after surgery, and spinal fusion was determined by manual palpation,

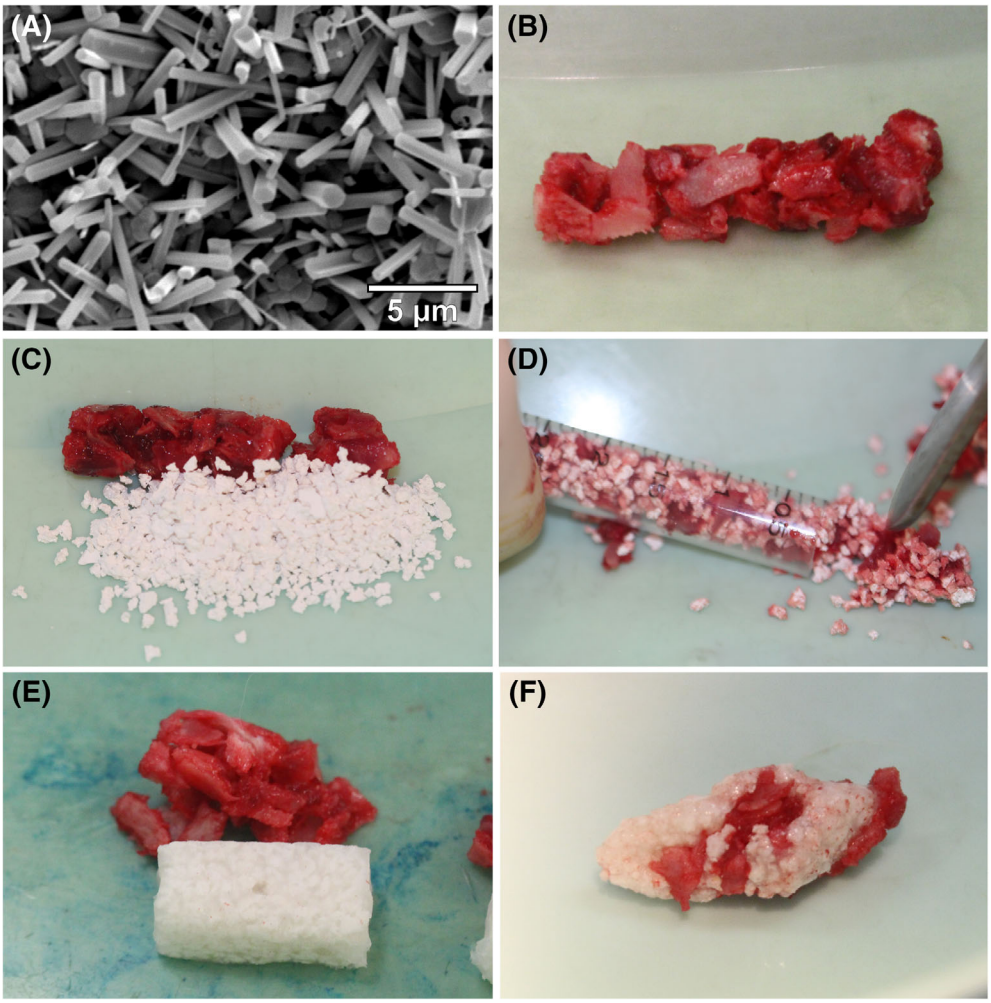

FIGURE 1. Graft materials used in PLF model, including (A) surface of submicron epitaxial polygon crystals observed on BCP granules by SEM, (B) iliac crest-derived autologous bone graft particles (ABG), (C, D) calcium phosphate granules and autograft particles combined in a 1:1 ratio ($ABG/BCP_{granules}$), and (E, F) granules embedded in polymeric carrier combined with autograft particles in a 1:1 ratio (ABG/BCP_{putty}).

radiography (Faxitron and micro-CT), mechanical testing (range of motion testing at 12 weeks only) and histology (decalcified and undecalcified). For the mechanical testing, five non-operated animals were included as baseline controls. For determining BCP material percentage in the implantation bed after surgery at time-point zero, 12 animals were used.

Radiographic analysis

Faxitron radiography. After harvesting the spines were immediately radiographed in the posteroanterior plane using a Faxitron (Faxitron Bioptics LLC, Arizona, USA) and digital plates (Agfa CR MD 4.0 cassette, Agfa, Germany). An Agfa Digital Developer and workstation was used to process the digital images (Agfa CR 75.0 Digitizer Musica, Agfa, Germany). The DICOM data was converted to bitmap images using DICOM Works (ezDICOM medical viewer, 2002). Radiographic status of the PLF was evaluated on the post-sacrifice anteroposterior faxitron radiographs utilizing the Lenke four-point grading scale.[29] A grade A was given to a fusion where it was deemed definitely solid with bilateral robust bridging bone. A grade B was given to a fusion where it was deemed probably solid with unilateral robust bridging bone and contralateral thin fusion mass. A grade C was given to a fusion where it was deemed probably not solid with a thin unilateral fusion mass and a probable pseudarthrosis on the contralateral side. A grade D was given to a fusion where it was deemed definitely not solid with thin fusion masses bilaterally with obvious pseudarthrosis or bone graft dissolution bilaterally. The occurrence of each grade (A–D) was determined based on faxitron image review by two independent observers blinded to treatment group and time-points.

Micro-computed tomography. Micro computed tomography (µCT) scanning was performed on all animals following radiography using an Inveon in-vivo micro computed tomography scanner (Siemens Medical, PA, USA) to obtain high-resolution radiographic images of the spinal fusions in three planes. Spines were scanned and the raw images reconstructed to DICOM data using Siemens software at a resolution of 53 microns. Images were examined in the axial, sagittal and coronal planes to assess the overall quality of

the fusion mass from transverse process to transverse process in a similar manner to the other radiographic data. Anterior and posterior 3D models were also created for each animal. The μCT reconstructions were assessed for fusion between the treated levels by two trained and experienced observers who reviewed the coronal and sagittal planes in a blinded manner to treatment groups and time-points. The μCTs were graded using the four-point Lenke radiographic grading score[29] as described above.

Manual palpation

Immediately after harvest, the stability of the lumbar spine of all animals was assessed by manual palpation according to Boden et al.[23] Two trained and experienced observers assessed the treated motion segment in a blinded manner in lateral bending and flexion/extension and compared it to the proximal and distal motion segments. The motion segments at L4–L5 were graded as either fused (rigid, no detectable movement at the disc space) or not fused (not rigid, movement detected at the disc space).

Biomechanical testing

Non-destructive range of motion testing was performed at 12 weeks to provide a kinematic, multidirectional flexibility analysis of the rabbit lumbar spine. Spines were tested with pure moments using a Denso robot (simVITRO; Cleveland Clinic BioRobotics Lab, Cleveland, OH) to avoid off axis moments and spurious loading. After fixing the spines in custom molds with resin, moments as per Grauer et al.[30] (270 *N*ċmm) were applied in axial rotation (AR), flexion-extension (FE), and lateral bending (LB). Moments of 270 *N*·mm were applied at a rate of 33.3 *N*·mm per second to a maximum of 300 *N*·mm, and was held for 15 s. A total of 4.5 load – unload cycles were run in each profile. The last three cycles were analyzed and a mean value at 270 *N*·mm was taken for each cycle and averaged. Range of motion testing was performed using robotic testing and intact, non-operated skeletally mature female rabbit spines (n = 5) that had no previous surgery were evaluated to provide a comparison.

Histology and histomorphometric analysis

All spines were immediately fixed for a minimum of 96 h in 10% formalin in 0.145 *M* phosphate buffered saline under gentle rotation, following mechanical testing. The spines were cut in the sagittal plane through the middle of vertebral body using a hacksaw and one side was randomly processed for decalcified paraffin histology and the other side processed for undecalcified polymethyl methacrylate (PMMA) histology. Decalcified histology was used to determine general tissue response and the presence of histological fusion. Undecalcified histology was used for the quantitative determination of bone formation and graft resorption.

Decalcified histology. The portion of the spines allocated for paraffin histology was decalcified in 10% formic acid in phosphate buffered formalin at room temperature for 3–4 days prior to further processing. The decalcified spines were then sectioned to provide detailed histology from the entire fusion mass from medial to lateral, which resulted in to at least four blocks from the treated spinal unit from transverse processes in the posterolateral fusion space. The blocks (~3 mm in thickness) were then embedded in paraffin and sectioned (5 microns) using a Leica Microtome (Leica Microsystems Pty Ltd, North Ryde, Australia). A minimum of three sections were cut from each paraffin block and stained with hematoxylin and eosin (H&E). Stained sections were examined in a blinded fashion (to treatment groups and time-points) using an Olympus light microscope (Olympus, Japan) with a DP72 high-resolution video camera (Olympus, Japan). Examination included qualitative assessment of general tissue response, the presence of inflammatory cells or tissue necrosis, evidence of graft resorption, new bone formation, marrow space development and bony fusion between both transverse processes. In addition, Rallis' Tetrachrome[31] staining was performed on decalcified sections in order to visualize bone maturation.

Undecalcified histology. The portion of the spines allocated for histomorphometric analysis was dehydrated through a series of ethanol and embedded in PMMA. A Leica SP1600 saw-microtome (Leica Microsystems Pty Ltd., North Ryde, Australia) was used to cut ~15 micron thick sections in the sagittal plane that were stained with methylene blue (Sigma, 1% in 0.1 *M* borax buffer, pH 8.5) and basic fuchsin (Sigma, 0.3% in water).[13] Three sections were cut from each PMMA block, with a ~2 mm interval to evaluate the entire fusion mass from medial to lateral. Low magnification images were used for histomorphometric analysis.

Histomorphometry. Three low magnification images (1.25×, 1 mm scale bar) taken from the transverse process, the middle of the fusion and the other transverse process were used for quantitative analysis. The region-of-interest (ROI) was determined by an observer blinded to treatment groups or time-points, using a polygon technique and graft material or bone tissue (mineralized bone and bone marrow elements) was identified by pixel color and morphology assessment. Their respective area was determined as a percentage of the ROI, and a mean value was obtained for each animal based on the three PMMA sections.

Statistical analysis

SPSS for Windows (SPSS, Chicago, IL) was used for statistical analysis. Fusion grading data were analyzed using a Kruskal–Wallis analysis of variance. Biomechanical testing data was analyzed using a one-way analysis of variance followed by a Games Howell post-hoc test when appropriate. Analysis of variance followed by a Games Howell post hoc test was performed on the histomorphometry data. Statistical significance was set at $p < 0.05$.

RESULTS

Surgery

Surgery was uneventful and no post-operative complications were observed. All animals ambulated normally throughout the study and were euthanized at their allocated time-points.

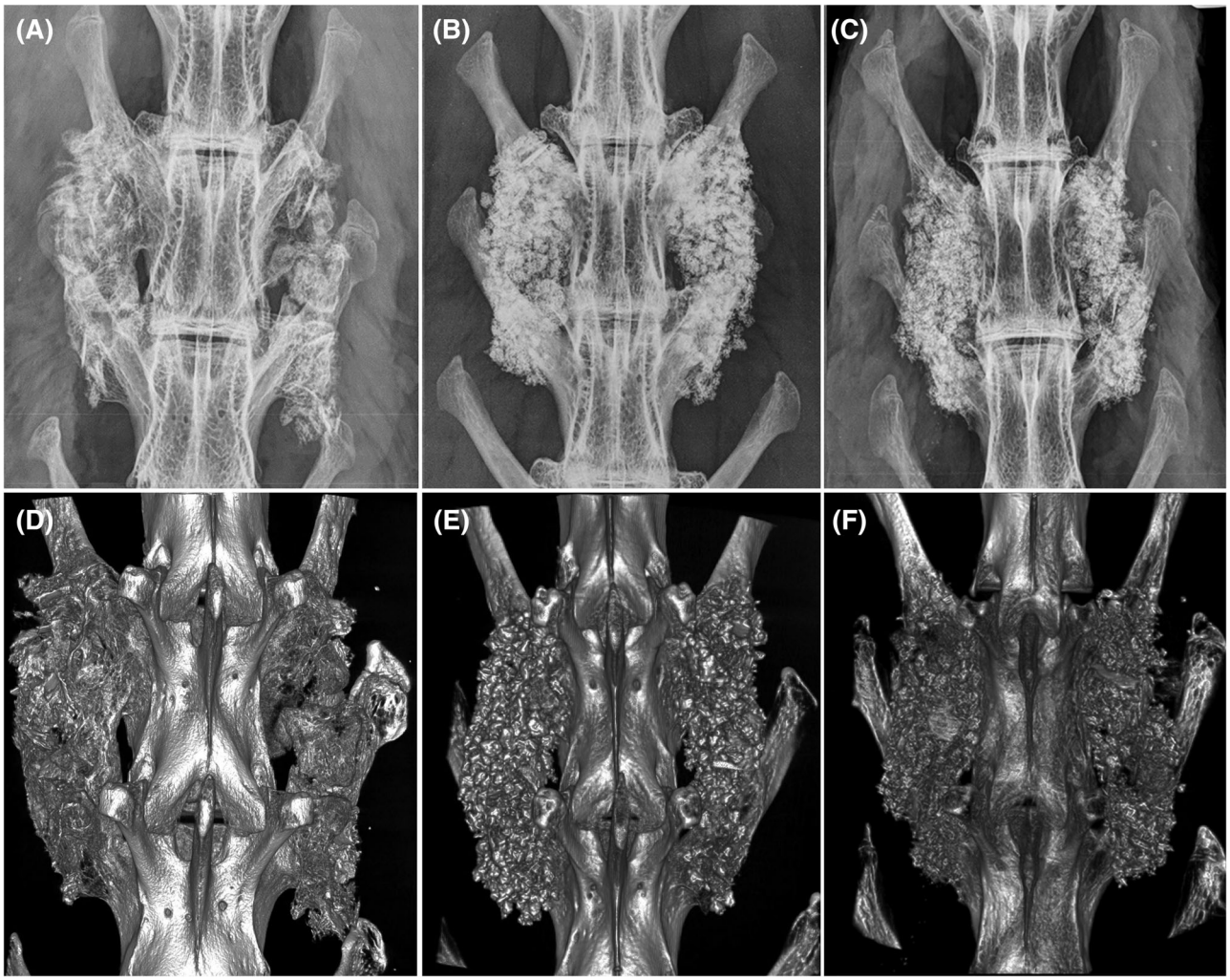

FIGURE 2. Radiography. (A–C) Examples of faxitron radiographs taken after 12 weeks for (A) ABG, (B), ABG/$BCP_{granules}$, and (C) ABG/BCP_{putty}. (D–F) Examples of 3D micro-CT reconstructions taken after 12 weeks for (D) ABG, (E), ABG/$BCP_{granules}$, and (F) ABG/BCP_{putty}. Faxitron radiographs and micro-CT reconstructions show the presence of graft material bridging the intertransverse process space of the treated levels in all groups.

Radiographic analysis

Post-operative radiographs demonstrated proper implantation position for all animals, which was maintained for all graft types for the entire study duration. No migration of BCP granules from the implantation site was observed for ABG/$BCP_{granules}$ and ABG/BCP_{putty} on radiographs and by micro-CT. For all groups, a progression in healing was observed during time. Radiographs showed the progression of a fusion mass with autograft and BCP particles with well-defined borders at 6 weeks toward a more homogeneous mass by 12 weeks for all groups [Fig. 2(A–C)]. By micro-CT, evidence of bone formation on the decorticated host bone transverse processes was observed at 6 weeks with all groups. During time, the autograft and BCP particles coalesced by new bone formation and bone remodeling, leading to solid fusion mass by 12 weeks for all groups [Fig. 2(D–F)]. Fusion grading was performed according to the Lenke scale on radiographs [Fig. 3 (B)] and micro-CT [Fig. 3(C)]. Grading distributions were similar between all groups at each time-point, with no statistically significant differences. A high occurrence of solid bilateral fusion (grade A) was determined after 12 weeks, corresponding to fusion rates of 75%, 87.5%, and 75% by radiography and 87.5%, 100%, and 87.5% by micro-CT for ABG, ABG/$BCP_{granules}$ and ABG/BCP_{putty}, respectively.

Manual palpation

Fusion assessment by manual palpation revealed a similar fusion distribution across groups at each time-point [Fig. 3 (A)]. At 6 weeks, bilateral fusion was determined in only one of five spines for both ABG/$BCP_{granules}$ and ABG/BCP_{putty}, while no fusion was observed for ABG. During time, fusion had increased to three of five at 9 weeks and six of eight at 12 weeks for all groups, corresponding to a fusion rate of 75% for the latest time-point. No statistically significant differences were determined between treatments.

Biomechanical testing

Results of range-of-motion (ROM) analysis measured after 12 weeks are presented in Table I. Non-operated control

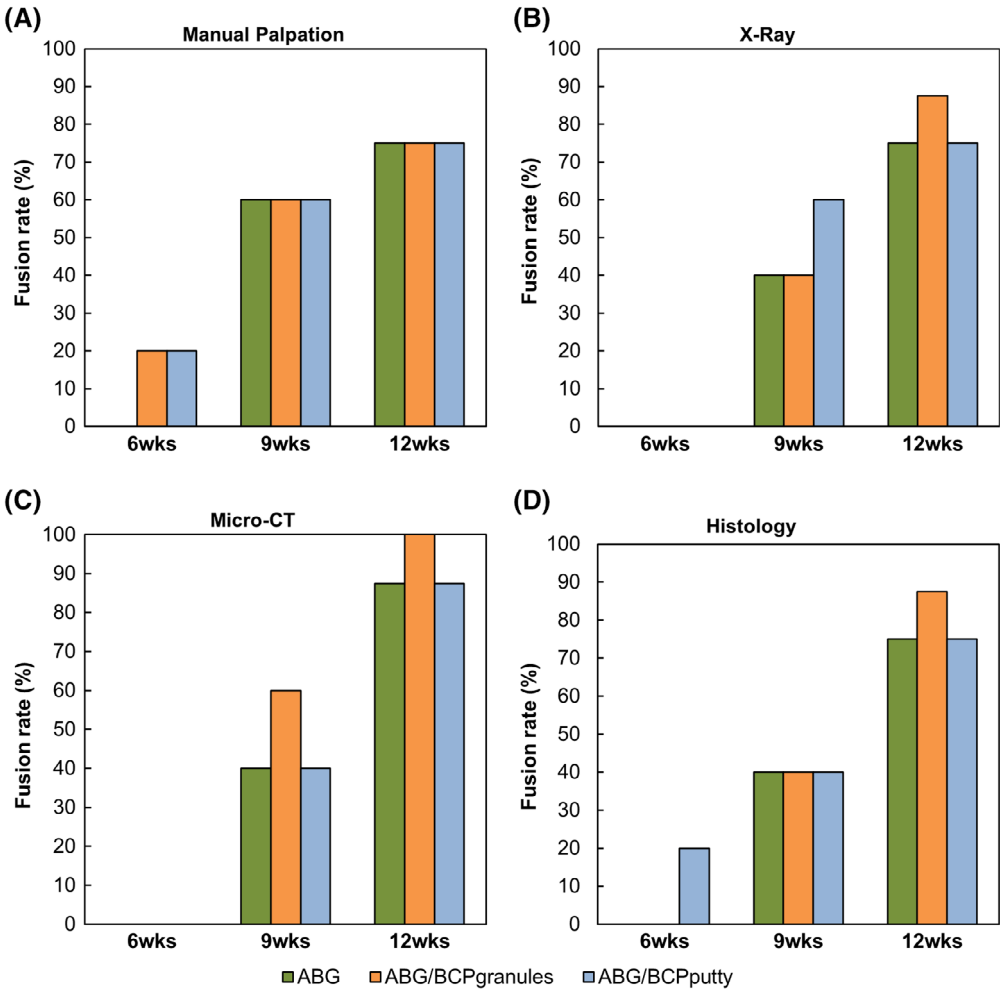

FIGURE 3. Diagrams presenting the fusion rate as determined by (A) manual palpation, (B) X-ray, (C) micro-CT, and (D) histology. For A and B, only the percentage of treated levels that achieved solid bilateral fusion (Lenke grade A) are shown. For all assessment methods, no significant differences in fusion rate between treatments were determined at all time-points.

TABLE I. Mean Range of Motion (°) of Treated Spine Levels in Response to Pure Moment Loading After 12 Weeks

Parameter	Control	ABG	ABG/$BCP_{granules}$	ABG/BCP_{putty}
Lateral bending	18.8 ± 1.9° ([a])	5.3 ± 2.2°	7.7 ± 3.9°	10.7 ± 2.1° ([b])
Flexion extension	20.7 ± 2.9° ([c])	8.0 ± 2.2°	7.9 ± 2.8°	11.6 ± 2.0° ([d])

Data presented in mean ± sd.
[a]Significantly different from all other groups, $p < 0.001$.
[b]Significantly different from ABG, $p < 0.001$.
[c]Significantly different from all other groups, $p < 0.001$.
[d]Significantly different from ABG, $p < 0.05$.

spines had a ROM of 18.8 ± 1.9 in LB and 20.7 ± 2.9 FE, indicating baseline ROM. With a difference of ±50% or more as compared to the controls, the ROM of treated spines in LB and FE after 12 weeks was significantly lower for all groups ($p < 0.001$). Between treatments, ROM of ABG and ABG/$BCP_{granules}$ were equivalent in both measuring movements, with no significant differences. Also, ROM between ABG/$BCP_{granules}$ and ABG/BCP_{putty} was similar in LB. For ABG/BCP_{putty}, ROM was slightly higher than other treatments in LB (ABG $p < 0.001$) and FE (ABG $p < 0.05$, ABG/$BCP_{granules}$ $p < 0.05$). There was no significant difference ($p > 0.05$) in axial rotation between the negative control (un-operated spine) and the positive control (autograft). Furthermore, there were no differences between the BCP treatments and either control.

Histology and histological grading

Histological observations are presented in examples of low-magnification overviews (Fig. 4) and high magnification micrographs (Figs. 5 and 6). On the histological overviews, fusion was determined in case of a bridge of bone tissue in the fusion mass connecting the adjacent transverse processes. By this method, fusion rates of 0–20% at 6 weeks,

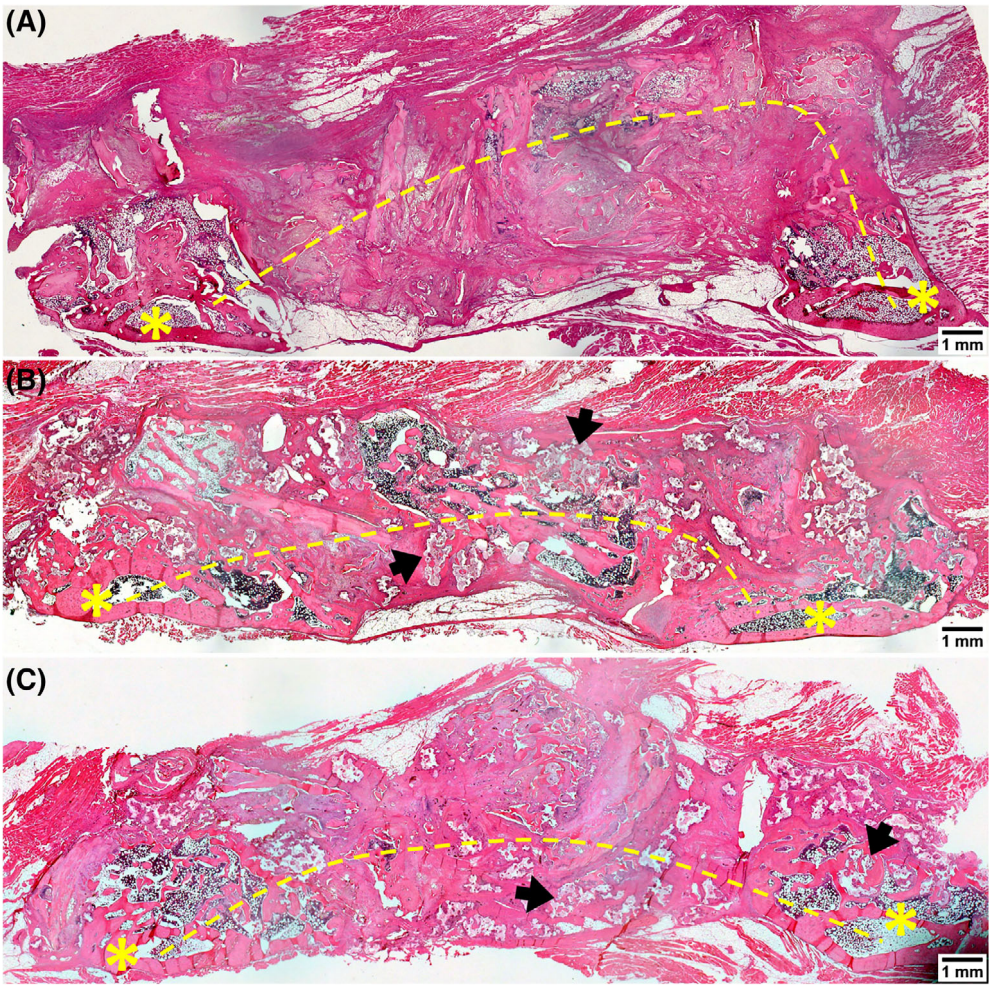

FIGURE 4. Histological panel overviews (H&E) of fusion masses of spines treated with (A) ABG, (B) ABG/$BCP_{granules}$, and (C) ABG/BCP_{putty} at 12 weeks post-surgery. All these fusion masses were determined to be fused, as indicated by the continuous bone mass (dashed line) between the adjacent transverse processes (yellow asterisks). The presence of calcium phosphate granules in the fusion mass was observed in the autograft extender groups (black arrows).

40% at 9 weeks and 75–87.5% at 12 weeks were determined, with no significant differences between graft types [Fig. 3(D)].

Histological micrographs showed the presence of residual particles, BCP granules and new bone formation with typical bone cells (Figs. 5 and 6). After 6 weeks, the formation of new bone on and between the BCP granules and the residual autograft particles was observed [Figs. 5(A,C) and 6 (A,B,D,E)]. New bone tissue at 6 weeks had infiltrated the BCP pores and was characterized by early, woven bone phenotype and fibrous tissue. Histology at 9 and 12 weeks showed healing progression by new bone formation and remodeling of bone into lamellar bone in and around the BCP material, as well as the development of bone marrow spaces with hematopoietic cells [Figs. 5(B,D) and6(C,F)].

Osteoblasts were observed typically lining the surface of new bone in the process of bone formation (Fig. 5) as well as osteocytes residing in lacunae. Multi-nucleated cells were present on the surface of the BCP material (Fig. 5), indicating foreign body giant cell- and osteoclast-mediated resorption of the material.

Histomorphometric analysis

Quantitative histomorphometry results of bone tissue and material in the fusion mass are presented in Figure 7. At all time-points, bone percentage was between 30% and 40% with no significant differences between groups and no trends being apparent over the different time-points. Regarding the percentage of BCP material, a gradual reduction in material percentage during time was apparent for both $BCP_{granules}$ and BCP_{putty}. However, the percentage of material for ABG/BCP_{putty} was significantly higher than for ABG/$BCP_{granules}$ at all time-points except time-point zero.

DISCUSSION

The objective of this study was to evaluate the performance of a novel BCP bone graft with submicron surface topography as an autograft extender against autograft alone in a validated model of PLF in rabbit. The BCP was applied either as granules or as granules embedded in a fast-dissolving polymeric carrier, both in combination with an equal volume of

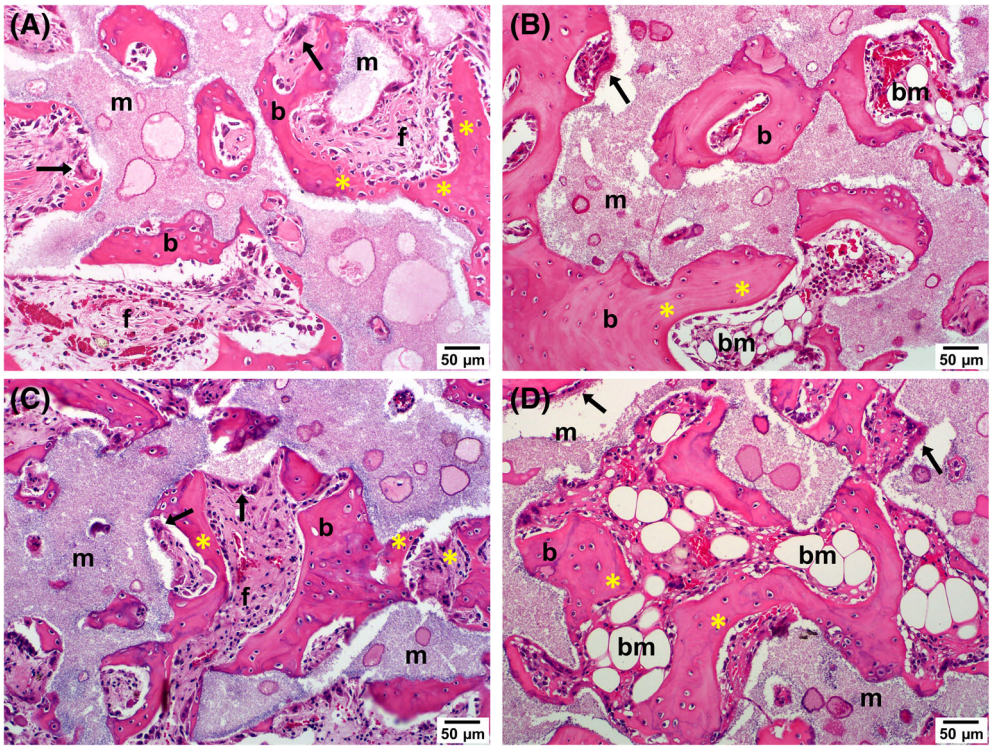

FIGURE 5. Histological micrographs (H&E) of the fusion masses of (A, B) ABG/$BCP_{granules}$ and (C, D) ABG/BCP_{putty} at (A, C) 6 weeks and (B,D) 12 weeks. At 6 weeks, bone tissue was characterized by woven bone and fibrous tissue and was observed at the material surface and inside of the pores. After 12 weeks, bone tissue had developed toward mature bone phenotype as determined by the presence of hematopoietic bone marrow spaces. Osteoblasts were observed depositing new bone matrix (yellow asterisks) and large, multi-nucleated cells were seen at the material surface resorbing material (black arrows). Legend: *m*: calcium phosphate material; *b*: bone; *f*: fibrous tissue; *bm*: bone marrow.

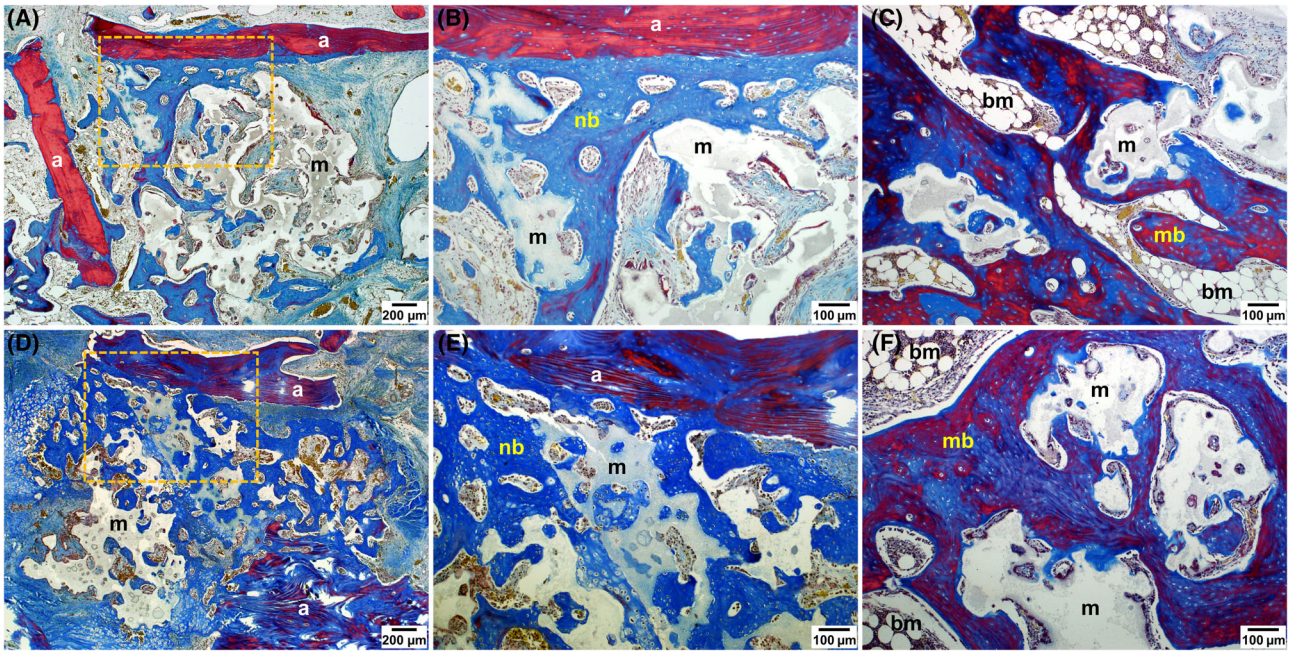

FIGURE 6. Histological micrographs (Tetrachrome) of the fusion masses of (A–C) ABG/$BCP_{granules}$ and (D–F) ABG/BCP_{putty} at (A, D; frames B, E) 6 weeks, and (C, F) 12 weeks. After 6 weeks, newly formed woven bone (blue) was observed growing from autograft particles, forming a direct connection between calcium phosphate granules and autograft particles. After 12 weeks, bone maturation was evident from the development of mature bone matrix (red) between granules as well as the presence of large bone marrow spaces. Legend: *a*: autograft particle; *m*: calcium phosphate material; *nb*: new bone; *bm*: bone marrow; *mb*: matured bone.

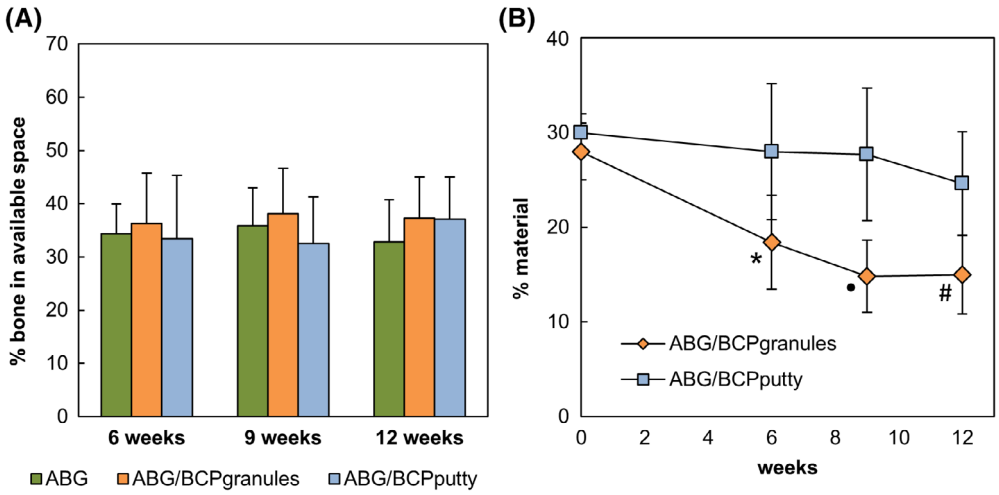

FIGURE 7. Diagrams presenting the results of histomorphometrical analysis, showing percentage of bone in available space (A) and material (B) in the fusion mass over time (means ± sd). Symbols: *significantly different from material, ABG/BCP_{putty}, 6 weeks $p < 0.01$; •significantly different from material, ABG/BCP_{putty}, 9 weeks $p < 0.001$; #significantly different from material, ABG/BCP_{putty}, 12 weeks $p < 0.001$.

autologous iliac crest bone. Outcomes were determined by an extensive range of assessment methods, including manual palpation, X-ray, micro-CT, mechanical testing, histology, and histomorphometry at endpoints of 6, 9, and 12 weeks post-surgery.

Based on all endpoints, all the three groups (ABG, ABG/$BCP_{granules}$, ABG/BCP_{putty}) showed a gradual progression in bone formation and maturation during time, leading to solid fusion masses between the transverse processes after 12 weeks. Results of fusion assessment by manual palpation, radiography (X-ray, microCT) and histology revealed equivalent fusion rates between all groups at all time-points, with satisfactory fusion rates after 12 weeks corresponding to literature.[23,32] Previous research has demonstrated that certain methods of fusion assessment (e.g., micro-CT) are more sensitive than other techniques (e.g., manual palpation, X-ray),[23,33] although each technique has advantages and disadvantages. Manual palpation and X-ray assessments are of a more subjective nature and allow global assessment of the fusion mass as compared to the high level of detail offered by micro-CT and histology. However, while histology is an excellent method to show bone formation, it is suboptimal for the assessment of fusion status as it may give false non-union results. A histological slide provides a two-dimensional representation of a more complex three-dimensional fusion mass and apparent non-contiguity between bone islands in a two-dimensional histological slide could still be contiguous in another plane. A disadvantage of fusion assessment by micro-CT (and X-ray) is that bone mineral and calcium phosphate-based graft materials have similar radiopacity, which can limit the ability to differentiate these components in a fusion mass. Despite all this, an advantage of preclinical investigation compared to the clinic is that multiple descriptive methods for fusion characterization can be used concurrently to develop a robust overall comparison between treatment outcomes. As expected, we noted variation in fusion rate depending on the analytical technique used, but our hypothesis that there would be no difference between autograft and BCP treatments was corroborated by each of the four analyses conducted.

In accordance with the fusion assessment results, mechanical testing of the spines after 12 weeks showed a substantially lower ROM (~50%) in LB and FE in all groups as compared to non-operated controls, indicating successful spinal fusion. There was no significant difference ($p > 0.05$) in ROM in LB or FE between the BCP treatments. There was more laxity for ABG/BCP_{putty} compared to ABG, but this did not correspond with a lower fusion rate using radiographical or histological methods. Moreover, there was no difference between groups when characterizing the volume of new bone formation by histomorphometry. Furthermore, a recent study in a sheep PLF model in which $BCP_{granules}$ and BCP_{putty} were implanted as stand-alone grafts and compared to an autograft positive control reported no difference in any mode of flexibility analysis.[34] We found no difference between the positive control, autograft, and the negative control, an un-operated spine, when tested in axial rotation in this study. This could be attributed either to the low sensitivity of the test method in this mode of flexibility or the possibility that more time was required to reach a complete fusion.

In line with the above results, histology and histomorphometry of the fusion mass showed the formation and maturation of bone tissue in the fusion mass during time in all groups, with typical bone morphology and bone-related cell types. Osteoclast-like, multinucleated cell-mediated were observed resorbing the BCP material, which are thought to play a role in the unique bone forming ability of calcium phosphates with submicron scale surface topography.[15]

Although the fusion rate evidently increased between 6 and 12 weeks post-surgery, the percentage of bone tissue in available space in the fusion mass as determined by histomorphometry remained stable (30–40%) in all groups during this period. This suggests that bone formation had reached an equilibrium at 6 weeks and thereafter, as new

bone formation was in balance with ongoing bone resorption and remodeling. Between 6 and 12 weeks, this process resulted in consolidation and maturation of the grafts into a stable fusion mass at 12 weeks. In retrospect, addition of an earlier time-point at 3 weeks post-surgery would have provided insight in the progress of bone formation before the equilibrium was reached. With regard to the calcium phosphate material in the fusion mass, the higher percentage of material in the ABG/BCP_{putty} group is likely the result of a higher density of granules in the implant bed related to implantation within the polymeric carrier, whereas granules implanted without carrier might become slightly more dispersed. However, this does not seem to have influenced fusion efficacy, as shown by the other assessment methods.

For the proper evaluation of autograft extender performance in this rabbit PLF model, the amount of autograft used in combination with the extender material is a critical factor. Indeed, several studies have noted the positive correlation between the amount of implanted autograft and the fusion rate.[27,28,35] By using a low quantity of autograft that is unable to achieve fusion by itself ($\pm$1 cc), the effect of an autograft extender on fusion success can be reliably evaluated (bone paucity model[27]). We have determined previously that 1 cc of autograft alone was not able to achieve spinal fusion [unpublished data], a finding that has also been reported by others[27,28] However, almost all studies on calcium phosphate autograft extenders that have claimed equivalence to autograft in this model have used quantities of autograft considerably larger than 1 cc combined with the extender.[36–39] This may lead to a significant overestimation of the effect of these materials because the volume of autograft might be sufficient to achieve fusion by itself, as was clearly demonstrated in a study by Miller et al.[28] In contrast, by use of 1 cc of autograft combined with 1 cc of BCP in the current study, we have unequivocally shown that this material with submicron surface topography is an effective autograft extender, since it enhanced the fusion success of 1 cc of autograft up to the level of the positive control (2 cc of autograft). These results suggest that calcium phosphates with submicron topography are highly effective bone graft materials for use in spinal fusion procedures.

It has been demonstrated that biomaterial surface properties can alter the phenotype of macrophages,[16–18] which are key modulators in the tissue response to medical implants. These plastic cells are known to differentiate into various subtypes in response to environmental cues. Typically, they are classified into two main subpopulations that have different functionality: the M1 macrophage, which is microbicidal and promotes an inflammatory response that can contribute to tissue injury, and the pro-healing, anti-inflammatory, M2 macrophage, which is involved in tissue repair and healing.[40] Although having opposing functions, the presence of both subpopulations is important for normal wound repair and also for the integration and healing of bone grafts.[40] Studies have suggested that an upregulation in anti-inflammatory M2 macrophages after a transient phase of inflammation dominated by M1 macrophages is crucial for enhanced vascularization and osteogenesis.[20,21] Recently, it has been shown that calcium phosphates with submicron surface topography promote naïve macrophages to adopt the M2 phenotype *in vitro*.[22] The promotion of M2 macrophages on submicron topographies might be the underlying mechanism behind the enhanced angiogenesis and bone healing observed with calcium phosphates with submicron topography *in vivo*.[11,14,22]

It should be mentioned that all pre-clinical studies are limited in the attempt to represent a model of a human scenario. The rabbit PLF model provides a biological bed to evaluate the in vivo performance of bone grafting options that may facilitate fusion. This model is limited in the anatomical and physiological differences between rabbit and human as well as the lack of fixation by instrumentation compared to human PLF. Although this study investigated calcium phosphates with submicron topography, no calcium phosphates without submicron topography were included as control. This would have allowed a more critical evaluation of the effect of submicron topography on bone graft performance in this model. Also, inclusion of additional time-points would have provided valuable information on the healing process, like the progression of bone formation early in the healing process (i.e., 3 weeks) and also the amount of remaining BCP material after a longer term of implantation (i.e., 26 weeks). A recommendation for future studies in this model is to include calcium phosphates with submicron topography as stand-alone grafts instead of autograft extenders, in order to evaluate the performance of these materials in the absence of autograft. However, recently, these materials have already shown potential as stand-alone grafts in an *Ovine* model of instrumented PLF.[34]

CONCLUSIONS

This study shows equivalent fusion rates between ABG and a novel synthetic BCP with submicron surface topography when used as a 1:1 graft extender in a single-level rabbit PLF model. Using an extensive range of evaluation techniques, a gradual progression of bone formation was determined, leading to high fusion rates after 12 weeks, with consistency between groups. Implantation of the BCP material within a fast-resorbing polymeric carrier did not affect treatment outcomes, indicating that the carrier did not inhibit the bone forming-ability of the material. By these findings, we can conclude that this novel BCP is a promising bone graft material for clinical spinal fusion procedures.

ACKNOWLEDGMENTS

This study was supported by the European Union's Horizon 2020 research and innovation program (grant agreement no. 674282). The authors are grateful to Dr. T. Wang (Surgical and Orthopedic Research Laboratories, University of New South Wales, Sydney, Australia) for his help with the ROM measurements.

REFERENCES

1. Dimar JR, Glassman SD, Burkus JK, Carreon LY. Clinical outcomes and fusion success at 2 years of single-level instrumented posterolateral fusions with recombinant human bone morphogenetic

protein-2/compression resistant matrix versus iliac crest bone graft. Spine 2006;31:2534–2539.
2. Dimar JR, Glassman SD, Burkus JK, Pryor PW, Hardacker JW, Carreon LY. Two-year fusion and clinical outcomes in 224 patients treated with a single-level instrumented posterolateral fusion with iliac crest bone graft. Spine J 2009;9:880–885.
3. Fischgrund JS, Mackay M, Herkowitz HN, Brower R, Montgomery DM, Kurz LT. Degenerative lumbar spondylolisthesis with spinal stenosis: A prospective, randomized study comparing decompressive laminectomy and arthrodesis with and without spinal instrumentation. Spine 1997;22:2807–2812.
4. Glassman SD, Dimar JR, Burkus K, Hardacker JW, Pryor PW, Boden SD, Carreon LY. The efficacy of rhBMP-2 for posterolateral lumbar fusion in smokers. Spine 2007;32:1693–1698.
5. Vaccaro AR, Lawrence JP, Patel T, Katz LD, Anderson DG, Fischgrund JS, Krop J, Fehlings MG, Wong D. The safety and efficacy of OP-1 (rhBMP-7) as a replacement for iliac crest autograft in posterolateral lumbar arthrodesis – A long-term (>4 years) pivotal study. Spine 2008;33:2850–2862.
6. Zdeblick TA. A prospective, randomized study of lumbar fusion. Preliminary results Spine 1993;18:983–991.
7. Banwart JC, Asher MA, Hassanein RS. Iliac crest bone graft harvest donor site morbidity. A statistical evaluation. Spine 1995;20: 1055–1060.
8. Rihn JA, Kirkpatrick K, Albert TJ. Graft options in posterolateral and posterior interbody lumbar fusion. Spine 2010;35:1629–1639.
9. Burger EL, Patel V. Calcium phosphates as bone graft extenders. Orthopedics 2007;30:939–942.
10. Nickoli MS, Hsu WK. Ceramic-based bone grafts as a bone graft extender for lumbar spine arthrodesis: A systematic review. Global Spine J 2014;4:211–216.
11. Habibovic P, Yuan H, van den Doel M, Sees TM, van Blitterswijk CA, de Groot K. Relevance of osteoinductive biomaterials in critical-sized orthotopic defect. J Orthop Res 2006;24:867–876.
12. Yuan H, van Blitterswijk CA, de Groot K, de Bruijn JD. A comparison of bone formation in biphasic calcium phosphate (BCP) and hydroxyapatite (HA) implanted in muscle and bone of dogs at different time periods. J Biomed Mater Res A 2006;78:139–147.
13. Yuan H, Fernandes H, Habibovic P, de Boer J, Barradas AMC, de Ruiter A, Walsh WR, van Blitterswijk CA, de Bruijn JD. Osteoinductive ceramics as a synthetic alternative to autologous bone grafting. Proc Natl Acad Sci U S A 2010;107:13614–13619.
14. Duan R, Barbieri D, Luo X, Weng J, de Bruijn JD, Yuan H. Submicron-surface structured tricalcium phosphate ceramic enhances the bone regeneration in canine spine environment. J Orthop Res 2016; 34:1865–1873.
15. Davison NL, Luo X, Schoenmaker T, Everts V, Yuan H, Barrère-De Groot F, de Bruijn JD. Submicron-scale surface architecture of tricalcium phosphate directs osteogenesis in vitro and in vivo. Eur Cell Mater 2014;27:281–297.
16. Bota PCS, Collie AMB, Puolakkainen P, Vernon RB, Sage EH, Ratner BD, Stayton PS. Biomaterial topography alters healing in vivo and monocyte/macrophage activation in vitro. J Biomed Mater Res Part A 2010;95A:649–657.
17. Hotchkiss KM, Reddy GB, Hyzy SL, Schwartz Z, Boyan BD, Olivares-Navarrete R. Titanium surface characteristics, including topography and wettability, alter macrophage activation. Acta Biomater 2016; 31:425–434.
18. Luu TU, Gott SC, Woo BWK, Rao MP, Liu WF. Micro- and nanopatterned topographical cues for regulating macrophage cell shape and phenotype. ACS Appl Mater Interfaces 2015;7:28665–28672.
19. Italiani P, Boraschi D. From monocytes to M1/M2 macrophages: Phenotypical vs. functional differentiation. Front Immunol 2014;5.
20. Loi F, Córdova LA, Zhang R, Pajarinen J, Lin TH, Goodman SB, Yao Z. The effects of immunomodulation by macrophage subsets on osteogenesis in vitro. Stem Cell Res. Ther 2016;7:15.
21. Spiller KL, Nassiri S, Witherel CE, Anfang RR, Ng J, Nakazawa KR, Yu T, Vunjak-Novakovic G. Sequential delivery of immunomodulatory cytokines to facilitate the M1-to-M2 transition of macrophages and enhance vascularization of bone scaffolds. Biomaterials 2015; 37:194–207.
22. Duan R, van Dijk LA, Luo X, Barbieri D, Pelletier M, Christou C, Rosenberg AJWP, Yuan H, Barrèrre-de Groot F, Walsh WR, de Bruijn JD Relation between macrophage differentiation, angiogenesis and topology-directed osteoinduction of calcium phosphate ceramics. In: Paper presented at: 64th Annual Meeting of the Orthopaedic Research Society, March 10–13, 2018; New Orleans, LA.
23. Boden SD, Schimandle JH, Hutton WC. An experimental lumbar intertransverse process spinal fusion model: Radiographic, histologic, and biomechanical healing characteristics. Spine 1995;20: 412–420.
24. Fredericks D, Petersen EB, Watson N, Grosland N, Gibson-Corley K, Smucker J. Comparison of two synthetic bone graft products in a rabbit posterolateral fusion model. Iowa Orthop J 2016;36:167–173.
25. Walsh WR, Oliver RA, Gage G, Yu Y, Bellemore J, Adkisson HD. Application of resorbable poly(lactide-co-glycolide) with entangled hyaluronic acid as an autograft extender for posterolateral intertransverse lumbar fusion in rabbits. Tissue Eng A 2011;17:213–220.
26. Walsh WR, Vizesi F, Cornwall GB, Bell D, Oliver RA, Yu Y. Posterolateral spinal fusion in a rabbit model using a collagen-mineral composite bone graft substitute. Eur Spine J 2009;18:1610–1620.
27. Curylo LJ, Johnstone B, Petersilge CA, Janicki JA, Yoo JU. Augmentation of spinal arthrodesis with autologous bone marrow in a rabbit posterolateral spine fusion model. Spine 1999;24:434–438.
28. Miller CP, Jegede K, Essig D, Garg H, Bible JE, Biswas D, Whang PG, Grauer JN. The efficacies of 2 ceramic bone graft extenders for promoting spinal fusion in a rabbit bone paucity model. Spine 2012;37:642–647.
29. Lenke LG, Bridwell KH, Bullis D, Betz RR, Baldus C, Schoenecker PL. Results of in situ fusion for isthmic spondylolisthesis. J Spinal Disord 1992;5:433–442.
30. Grauer JN, Erulkar JS, Patel TC, Panjabi MM. Biomechanical evaluation of the New Zealand white rabbit lumbar spine: A physiologic characterization. Eur Spine J 2000;9:250–255.
31. Rallis Z, Watkins G. Modified tetrachrome staining method for osteoid and defectively mineralized bone in paraffin sections. Biotech Histochem 1992;67(6):339–345.
32. Pelletier MH, Oliver RA, Christou C, Yu Y, Bertollo N, Irie H, Walsh WR. Lumbar spinal fusion with b-TCP granules and variable *Escherichia coli*–derived rhBMP-2 dose. Spine J 2014;14:1758–1768.
33. Goldstein C, Drew B. When is a spine fused? Injury 2011;42(3): 306–313.
34. van Dijk LA, Duan R, Luo X, Barbieri D, Pelletier M, Christou C, Rosenberg AJWP, Yuan H, Barrère-De Groot F, Walsh WR, de Bruijn JD. Biphasic calcium phosphate with submicron surface topography in an *Ovine* model of instrumented posterolateral spinal fusion. JOR Spine 2018;1(4):e1039.
35. Ghodasra JH, Daley EL, Hsu EL, Hsu WK. Factors influencing arthrodesis in a rabbit posterolateral spine model with iliac crest autograft. Eur Spine J 2014;23:426–434.
36. Fredericks DC, Petersen EB, Sahai N, Corley KG, DeVries N, Grosland NM, Smucker JD. Evaluation of a novel silicate substituted hydroxyapatite bone graft substitute in a rabbit posterolateral fusion model. Iowa Orthop J 2013;33:25–32.
37. Pugely AJ, Petersen EB, DeVries-Watson N, Fredericks DC. Influence of 45S5 bioactive glass in a standard calcium phosphate collagen bone graft substitute on the posterolateral fusion of rabbit spine. Iowa Orthop J 2017;37:193–198.
38. Smucker JD, Petersen EB, Fredericks DC. Assessment of MASTERGRAFT PUTTY as a graft extender in a rabbit posterolateral fusion model. Spine 2012;37(12):1017–1021.
39. Smucker JD, Petersen EB, Nepola JV, Fredericks DC. Assessment of Mastergraft(®) strip with bone marrow aspirate as a graft extender in a rabbit posterolateral fusion model. Iowa Orthop J 2012;32:61–68.
40. Klopfleisch R. Macrophage reaction against biomaterials in the mouse model – phenotypes, functions and markers. Acta Biomater 2016;43:3–13.